

## Using Weibull probability distribution to calibrate prevailing wind applying in oil spill simulation

**M. A. Badri\***  
Assistant Professor

*In the Persian Gulf, the major source of oil pollution is related to the transportation of tankers, offshore production and discharges by coastal refineries. The water dynamical field has been obtained using a new hydrodynamic model. Local wind is recognized as the principal driving force combining to the water dynamic field to determine oil drift on the sea surface. The Weibull probability distribution is considered to adjust the prevailing wind obtaining by data from measurements and compared with other data, displaying fairly good conformity. To model the advection and dispersion in the Persian Gulf which is a shallow water area, random walk technique has been used. Comparison of the actual and simulated oil spill trajectory based on real wind field was found acceptable in the Iranian waters.*

**Keywords:** Weibull distribution, Probability wind field, oil spill modeling, Persian Gulf

### 1 Introduction

The control over properties and behavior of fluid flow and relative parameters are the advantages offered by Computational Fluid Dynamics which makes it suitable for the simulation of the applied engineering problems [1]. Over the past three decades simplified empirical formulae contributed greatly in a rapid evaluation of the pollutant dynamics spreading and drifting. Modern models can utilize more accurate and physically relevant mathematical formulations. In the majority of cases, a mathematical modeling may be a strong and available tool not only for a rapid computation of the pollutant fate but for simulation of the various cleanup operations as well [2]. The computer simulation of complicated marine environment problems has become one of the interesting areas of the research works by development of efficient and accurate numerical methods suitable for the complex flow domain. Numerical models are widely used as an important component of contingency planning and coastal management. Such models act as a real time prediction tool to support in combating and prediction of contaminant movement in order to preserve the region's coastal resources.

The step of choosing the model is informed by experience, personal intuition and a degree of explicit dynamical reasoning. It is important to emphasize that once the model is chosen, the proper tests of its usefulness can come from the systematic, logical and precise working out

---

\* Assistant Professor, Subsea R&D centre, Isfahan Univ. of Tech., Isfahan, [malbdr@cc.iut.ac.ir](mailto:malbdr@cc.iut.ac.ir)

of the dynamical predictions of the laws of motion applying to the model. Numerical solution of the time-dependent advection/diffusion/decay equation may be obtained in two ways:

- By finite-difference or finite element approximations
- By the simulation of the continuum of dispersed contaminant by a cloud of discrete particles or 'particle-tracking' method

Particle tracking technique is preferable in the cases of higher dimensions, relatively few particles and where the contaminant cloud does not occupy the whole model. The particle tracking technique offers an efficient alternative as the processes of diffusion and decay generally require stochastic methods. Prediction of the motion of patches of surface oil and prediction of a thermal discharge from a power plant are examples using in particle-tracking technique [3]. This is because 'random-walk' method is selected here, as turbulent diffusion in these processes is generally simulated by this method.

One of the important applications of using hydrodynamic models is to provide cost-effective and reasonable estimates of oil surface drift and predict transport and fate of the oil slicks. Therefore, this model is suggested for consideration a model of the real ocean whose validity is examined for the Persian Gulf. The Persian Gulf region is well known as the most active oil production region in the world. Although, some extensive studies related to the oil spill have been published for the Persian Gulf [4-10], it still needs to some improvements and modifications and speed up procedures as well. These researches for the Persian Gulf have been included providing hydrodynamic Atlas, simulation and validation of some documented events. Also providing oil spill hazard contour maps for the prediction of oil spill travel time based on critical sea conditions are the outcomes [11-12].

In this work, the dynamical field is determined based on Kelvin propagation wave theory as a new hydrodynamic model and calibrated by measurements. Wind data on each grid has determined by synoptic stations and interpolated by Cressman analysis. Then, by using Weibull probability distribution wind field, prevailing wind on whole region is determined and calibrated. The advantages of the simple model are then applied for oil spill modeling. The important short term processes in the mathematical expression of spreading, dispersion and decay are considered. The Lagrangian approach has been used to describe the transportation of spilled oil. The suggested procedure is an attempt to find a simple way towards taking advantage of developments in environmental Modeling. Governing equations are verified and applied in the Persian Gulf to provide the capability of simulating a hypothetical oil spill accidents leading to oil spill hazard contour maps.

## 2 Governing equations

The  $kh$  parameter which is usually introduced to measure the strength of the depth, shows that the Persian Gulf has the condition of shallow water considering its overall latitude at  $\phi = 27^\circ$ . Where,  $k$  is the wave number modulus and  $h$  is mean depth [13]. Therefore, shallow water range  $kh < 0.7$  is considered. The governing equations are provided by the shallow water horizontal equations:

$$\frac{\partial h}{\partial t} + \frac{\partial}{\partial x}(hu) + \frac{\partial}{\partial y}(hv) = 0 \quad (1)$$

$$\frac{\partial u}{\partial t} + u \frac{\partial u}{\partial x} + v \frac{\partial u}{\partial y} - fv = -g \frac{\partial h}{\partial x} \quad (2)$$

$$\frac{\partial v}{\partial t} + u \frac{\partial v}{\partial x} + v \frac{\partial v}{\partial y} + fu = -g \frac{\partial h}{\partial y} \quad (3)$$

Where  $f$  is coriolis factor ( $f = 2\Omega \sin \phi$ ),  $\Omega$  is the angular velocity of earth and  $\phi$  is the latitude,  $h = h_0 + \eta$ ,  $\eta \ll h_0$  and  $g$  is the acceleration of gravity. The linearized form which ignores all quadratic terms in the dynamical variables is considered [14]. By manipulation of the momentum equations and using mass conservation equation, the governing equation becomes:

$$\frac{\partial}{\partial t} \left\{ (\partial^2 / \partial t^2 + f^2) \eta - C_0^2 \nabla^2 \eta \right\} = 0 \quad (4)$$

where  $c_0$  is wave propagation velocity. Wave solution which is periodic in  $x$  and  $t$  can be sought by  $\eta = \text{Re } \bar{\eta}(y) e^{i(kx - \sigma t)}$ . Where  $\bar{\eta}(y)$  is the complex wave amplitude which varies with the coordinate  $y$ . In rigid boundaries, velocity in  $y$ -direction must vanish, which implies  $\partial^2 \eta / \partial y \partial t - f \partial \eta / \partial x = 0$  (at  $y = 0, L$ ). The eigen value relation using boundary conditions at  $y=0$  &  $y=L$  yields  $(\sigma^2 - f^2)(\sigma^2 - C_0^2 k^2) \sin \alpha L = 0$ . The solution plays the role of  $n=0$  mode due to the effects of the rotation, in case  $\sigma^2 = C_0^2 k^2$  it names Kelvin waves. Where  $\sigma = C_0 k$  is wave angular frequency. Consider a long straight coast line  $y=0$  in the northern hemisphere with water at its left side and a sample wave traveling along this boundary. Due to the rotation of the earth, the water level builds up at the coast, which results in a greater wave amplitude nearer the coast. Thus leads to a pressure gradient which balances the rotational force. The wave resulting from this is called a Kelvin waves. Kelvin waves are special solutions of the small amplitude linearized inviscid depth-averaged shallow water equations, i.e. [14]:

$$\frac{\partial \eta}{\partial t} + \frac{\partial(uH_0)}{\partial x} + \frac{\partial(vH_0)}{\partial y} = 0; -\infty < x < +\infty, y = 0 \quad (5)$$

$$\frac{\partial u}{\partial t} - fv = -g \frac{\partial \eta}{\partial x} \quad (6)$$

$$\frac{\partial v}{\partial t} + fu = -g \frac{\partial \eta}{\partial y} \quad (7)$$

Satisfying the boundary conditions  $v = 0$ ; at  $y = 0$ . It also satisfies the condition that the wave amplitude is decaying away from the coast. In relations (5, 6 and 8)  $\eta$  denotes the surface elevation with respect to the reference plane,  $u$  and  $v$  are the horizontal depth-averaged velocity components. In order to determine the Kelvin wave, one may consider the trial solution.

$$\eta = f_1(y) e^{\pm i(kx - \sigma t)}, u = f_2(y) e^{\pm i(kx - \sigma t)}, v = f_3(y) e^{\pm i(kx - \sigma t)} \quad (8)$$

The functions  $f_1, f_2, f_3$  are determined such that this trial solution solves the differential equations and satisfies the conditions put forward. Some lengthy computations show  $f_1, f_2, f_3 \propto e^{-\beta y}$  and algebraic equations for the parameters imply  $f_3 = 0$ ,  $\sigma^2 = C_0^2 k^2$ ,  $\beta = f / C_0$  ( $C_0 = \sqrt{gH_0}$ ). As a result, the Kelvin wave, written in its most compact form, reads:

$$\eta = \eta_0 e^{-\frac{f}{C_0} y} \cos[k(x \pm C_0 t) + \varphi], u = \sqrt{\frac{g}{H_0}} \eta, v = 0 \quad (9)$$

For a Rossby radius  $R = C_0 / f$  from the coast line ( $y=0$ ) the amplitude has fallen to  $0.37\eta_0$  (Pugh-1996). In practice, Kelvin waves are most important for describing tidal amplitudes in

presence of long coast lines. In the Persian Gulf, the open connection with the Indian Ocean at the Strait of Hurmoz will basically travel into the Persian Gulf as Kelvin waves under presence of the north-east coastal line. Fig.1 presents the approximate setting taken to describe the Kelvin wave. In fact, the plane of the domain is rotated at  $\theta = 25.9$  in order to fit the domain to the new coordinate system  $(x', y')$  and setting the coastlines nearly parallel to the new horizontal coordinate  $x'$ . Also this direction is nearly towards the prevailing wind direction in the Persian Gulf. Without loss of generality it is possible to consider only one of the modes from (12) and the Kelvin wave taken reads:

$$\eta = \eta_0 e^{-\frac{f}{C_0} y'} \cos[k(x' - C_0 t) + \varphi], \quad u' = \sqrt{\frac{g}{H_0}} \eta, \quad v' = 0 \quad (10)$$

Here,  $x', y'$  are coordinates in a rotated frame (Fig. 1) and  $u', v'$  are the velocity components with respect to the rotated frame. To accomplish expressions in the  $x, y$ -coordinate system it needs to be observed that:

$$\begin{bmatrix} x \\ y \end{bmatrix} = M \begin{bmatrix} x' \\ y' \end{bmatrix}, \quad \begin{bmatrix} u \\ v \end{bmatrix} = M \begin{bmatrix} u' \\ v' = 0 \end{bmatrix}, \quad M = \begin{bmatrix} \cos \theta & \sin \theta \\ -\sin \theta & \cos \theta \end{bmatrix} \quad (11)$$

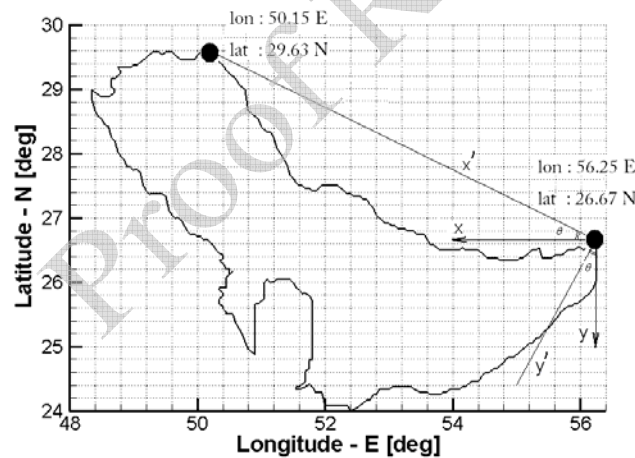


Figure 1 Rotation of plane of the domain

### 3 Kelvin wave expansions

The atmosphere and the ocean have so many fluid-dynamical properties in common that the study of one often enriches our understanding of the other. Experience has also shown that the recognition of the underlying dynamical concepts applicable to both the atmosphere and the oceans is an excellent starting point for the study of either. Geophysical fluid dynamics is the subject whose concerns are the fundamental dynamical concepts essential to understanding of the atmosphere and the oceans. In principle, geophysical fluid dynamics deals with all naturally occurring fluid motions. Such motions are present on an enormous range of spatial and temporal scales. It is on large scales that the common character of

atmosphere and oceanic dynamics is most evident, while at the same time the majestic nature of currents due to tides, gulf streams makes such a focus of attention emotionally compelling and satisfying. In practice, measurements extend over finite periods, often a year, a month or even a few days and so the results from analyzing these finite lengths of data can only approximate the true constants. Sea surface level, currents, atmospheric pressure and earth movements are usually referred as periodic and regular motions. Any sequence of measurements for sea-level or currents has a tidal and non-tidal component. In order to describe tidal patterns without applying elaborate analysis procedure, it is possible to determine tides as time series according to basic statistics. The general representation of the observed level  $Z(t)$  varying with time may be written as  $Z(t) = Z_0(t) + T(t) + S(t)$ .  $T(t)$  is the tidal part of the variation and  $S(t)$  is the meteorological surge component. For tidal data analysis, there are two sets of measurements called sea levels and currents which can be measured and conveniently tabulated. A further extremely useful technique called Fourier analysis represents a time series in terms of the distribution of its variance at different frequencies. The basic idea of Fourier analysis is that any function which satisfies certain theoretical conditions may be represented as the sum of a series of sines and cosines of frequencies which are multiples of the fundamental frequency  $\sigma_M = \frac{2\pi}{M \cdot \Delta t}$ . Where,  $M$  is the number of observations of the variable  $Z(x, y, t)$  in the time interval. The theoretical conditions required of the function  $Z(x, y, t)$  are satisfied by any series of observations of natural phenomena. Here, the function  $Z(x, y, t)$  is satisfied by sea levels and currents using similar expansion. It may be written as an application [15]:

$$Z(x, y, t) = Z_0 + \sum_{j=1}^{M/2} \eta_j(x, y) \cdot \cos(j\sigma_M t - \varphi_j(x, y)) \quad (12)$$

where,  $Z_0$  is the average value of  $Z_0(x, y, t)$  over the period of observations in each location and  $\eta_j(x, y)$  and  $\varphi_j(x, y)$  are the amplitude and phase of the  $j$ th harmonic constituents of  $Z(x, y, t)$ . In this work, a similarity between Fourier analysis as a time series and the tidal potential term, which can be used for any region, is invoked. It is expressed as a series with each term representing a tidal constituent.

In particular, it is known that the waves entering the Persian Gulf at the Strait of Hurmuz will carry the associated frequencies of which the data are given in table (1). In this table  $T$  and  $k = \frac{2\pi}{\lambda} = \frac{2\pi}{T\sqrt{gH_0}}$  is the period and the wave number of each constituent respectively.

**Table 1** Specifying the periods and wave numbers of the main constituents

	$M_2$	$S_2$	$K_1$	$O_1$
T [hr]	12.42	12.00	23.93	25.85
$k \times 10^6 [m^{-1}]$	7.58	7.85	3.94	3.64

According to shallow water equations for the Persian Gulf and by ignoring the quadratic terms, Kelvin wave theory is invoked (section 2). Through this procedure, the geo-physical effects and the domain constraints are considered as well. It can be mentioned that this procedure can be used for any region, if main constituents for tidal motion are known. These information named co-amplitude and co-phase lines are recorded in Admiralty tide tables and up-dated annually.

It is well-known that the main constituents for tidal motion are the principal semi-diurnal lunar and solar tides  $M_2, S_2$  and the principal diurnal tides  $K_1$  and  $O_1$ . The four main constituents are numbered with  $j=1, 2, 3, 4$ . Here,  $j=1$  corresponds with  $M_2$ ,  $j=2$  with  $S_2$ ,  $j=3$  with  $K_1$  and  $j=4$  with  $O_1$ . All four constituents introduce a Kelvin wave, traveling into the Persian Gulf with elevation:

$$\eta_j = \eta_{0j} e^{-\frac{f}{C_0} y'} \cos[k_j(x' - C_0 t) + \varphi_j] \quad (13)$$

Taking all four together we obtain as an approximate flow model the following Kelvin wave expansion:

$$\eta = Z_0 + \sum_{j=1}^4 \eta_j, \quad u' = \frac{C_0}{H_0} \sum_{j=1}^4 \eta_j, \quad v' = 0 \quad (14)$$

With respect to the surface elevation, it has been found that the success of the expansion hinges on the introduction of  $Z_0$  as an innovation can be used for any region. It contains a mean constant level taking the main effects of other sources into account. The mean surface level  $Z_0$ , is determined using the following relation for the Persian Gulf after some case studies.

$$Z_0 = 0.15 + \sum_{j=1}^4 \tilde{\eta}_{0j} \quad (15)$$

The value 0.15 is taken by considering seasonal streams.  $\tilde{\eta}_{0j}$  is the value of the main constituents before normalizing them. In order to finalize the expansion, the coefficient  $\eta_{0j}$  and  $\varphi_j$  need to be determined and this has been done point wise using the data provided by the admiralty tables. These parameters have been calculated for all grid points and are compared with the available data at four reference locations i.e. Kish and Siri islands and Bandar abbas and Bushehr ports for verification.

The admiralty tables contain charts of co-amplitude and co-phase lines based on time-averaged data. Using the charts, we have determined the amplitudes and phases of each of the main constituents in the grid points of the coarse grid,  $0.25^\circ \times 0.25^\circ$ . As an example, table (2) specifies  $\eta_{0j}$  and  $\varphi_j$  for a grid point close to Kish Island. In the next step, values of  $\eta_{0j}$  are normalized according to some trial and error procedures and for final flow estimation,  $\eta_{0j}$  is picked up from the normalized table (table 3). The coarse grid is much coarser than grids used for computational reasons later on. These finer grids are in general obtained by refinement of the coarse grid ( $3' \times 2.5'$ ). In order to obtain  $\eta_{0j}$  and  $\varphi_j$  on the fine grid as well, a simple bilinear interpolation is employed. For completeness of the procedure, it is necessary to present values of  $\eta_{0j}$  and  $\varphi_j$  in some of the land points of the coarse grid and we have just taken zero values for this aim. This implies that our procedure, very close to the boundaries is not accurate. However, against the background of the more global character of the present study, this was found acceptable.

**Table 2** Specifying the phase and amplitude of main constituents for the Kish Island

constituents	$M_2$	$S_2$	$K_1$	$O_1$
$\varphi_j$ : <i>ph.</i> [deg]	35.300	69.700	145.310	99.070
$\eta_{0j}$ : <i>amp.</i> [m]	0.350	0.140	0.333	0.200

**Table 3** Normalizing the amplitudes and phases for the Kish Island

Normalized constituents	M <sub>2</sub>	S <sub>2</sub>	K <sub>1</sub>	O <sub>1</sub>
$\varphi_j : ph.[deg]$	1.000	1.991	4.152	2.831
$\eta_{0j} : amp.[m]$	1.000	0.400	0.951	0.571

#### 4 Wind speed data

Table (4) includes the data used in the analysis. This table contains information about wind speed with the corresponding probability (measured 10 meters above the sea level). These data were analyzed by using the two-parameter Weibull distribution which adequately fit the data.

**Table 4** Wind speed data

Wind velocity [m/sec]	probability
0-4	33%
5-9	50%
10-14	15%
>15	2%

Weibull distribution is more appropriate for survival analysis, extreme value theory, weather forecasting, reliability engineering and failure analysis. However, both terminologies have been used in researches in this area, the method used by authors is more applicable for particle tracking and spill analysis. Here, the Weibull probability density function (pdf) of a random variable  $V$ , with parameters  $A_p$  and  $C_p$  is used mathematically. In this case  $V$  is a wind speed expressed in [m/sec]:

$$f(V; A_p, C_p) = (C_p / A_p) \cdot (V / A_p)^{C_p - 1} \exp[-(V / A_p)^{C_p}], V \geq 0, A_p, C_p > 0 \quad (16)$$

$A_p$  is a scaling parameter also in [m/sec] and  $C_p$  is a dimensionless shape parameter. The cumulative distribution function (cdf) [16] is obtained by:

$$P(V; A_p, C_p) = 1 - \exp[-(V / A_p)^{C_p}] \quad (17)$$

To estimate the parameters of Weibull, the least-squares approach is used. In order to obtain a linear problem, an expression of the below form is minimized:

$$1 - p = \exp[-(V / A_p)^{C_p}] \quad (18)$$

In other words, it is required to minimize  $\sum_{j=1}^k (\varepsilon)^2 = \sum_{j=1}^k \{[\ln(A_p^{-C_p}) + C_p \ln V_j - b_j]^2\}$ , where  $b_j = \ln\{-\ln[1 - p(V_j)]\}$  and  $K$  is the number of points we use to fit the curve. Because the data is not a vector of observations of wind speed, but is intervals with probabilities, the definition of Weibull distribution is used to estimate the parameters  $A_p$  and

$C_p$ . In other words, from the data it is possible to perform a set of probabilities which gives  $R_1$  as the vector of probabilities:

$$R_1 = \left[ p(0 \leq V < 4) \quad p(4 < V \leq 9) \quad p(9 < V \leq 14) \quad p(V > 14) \right]^T \quad (19)$$

The measured data provides another vector of probabilities called  $R = [0.33 \quad 0.50 \quad 0.15 \quad 0.02]^T$ .

The parameters  $A_p$  and  $C_p$  has been determined such that the difference between vector R and vector R1 is minimum. In other words, the function  $g(A_p, C_p) = \|R - R_1\|^2$  has been minimized. Therefore,  $A_p$  and  $C_p$  obtained as  $C_p = 1.7243$ ,  $A_p = 6.8005$ . To check if these parameters are good enough, the vector  $R_1 = [0.33 \quad 0.54723 \quad 0.16660 \quad 0.02]^T$  is calculated once again in table (5). As it can be seen, the difference between vector R and R1 is quite small and is in order of magnitude around  $10^{-2}$ . Therefore, Weibull probability density function can be determined by  $f = 0.06325V^{0.7243} \exp[-(V/6.8005)^{1.7243}]$ . The mean and standard deviation are:

$$\bar{V} = A_p \Gamma(1 + (1/C_p)) = 6.8005 \Gamma(1.57995) = 6.06 \quad (20)$$

$$\sigma^2 = A_p^2 [\Gamma(1 + (2/C_p)) - \Gamma^2(1 + (1/C_p))] = 13.0882 \quad (21)$$

Therefore, Mean = 6.06 and Standard Deviation = 3.618 has been considered for the wind distribution.

**Table 5** Deviation between calculation and actual wind data

items	R	R1	Dev. (%)
1	0.33	0.33	0.0
2	0.50	0.54723	9.4
3	0.15	0.1666	11.1
4	0.02	0.02	0.0

Figures (2) and (3) show the Weibull probability density time series and wind velocity distribution respectively to be used in oil spill model. By using Weibull distribution, the prevailing wind over the whole domain is calculated 5.196 [m/sec] which is very close to 5.26 [m/sec] from documented data with 1.2% deviation. Table (4) is shown the local deviation in some sample locations.

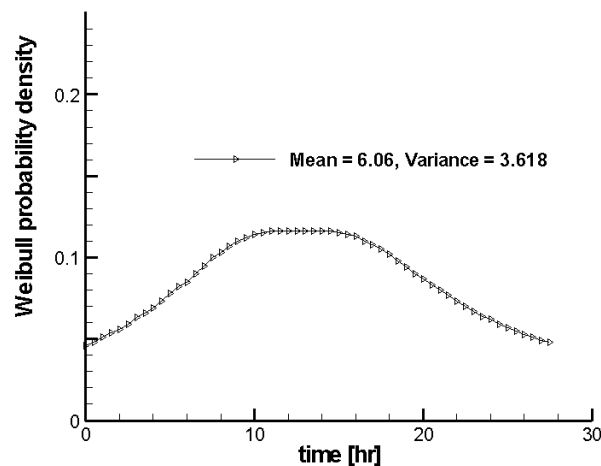


Figure 2 Weibull probability density time series

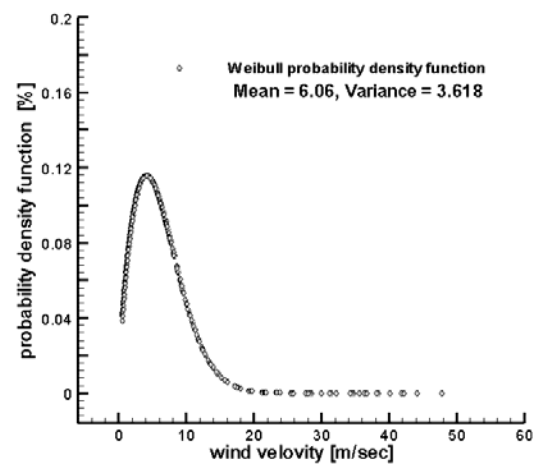


Figure 3 Weibull probability density function

## 5 Preparing a data base to be used to modeling

In this work, some of the important short-term processes have been considered and a portal has been provided to be used in a developed numerical model. Weathering data in the interval of the accident were prepared and imposed to the hydrodynamic model to simulate the trajectory and to determine oil slick surface and thickness. An analytical wind field has been generated by Weibull distribution and calibrated by means of data from the European Center for Medium-Range Weather Forecast (ECMWF) and data from Iranian synoptic stations with fairly good conformity (table 6). To compare the wind data on whole grid, Cressman analysis has been used as well. The wind velocity has been extended to the grid points considering the curvature of the earth and the value of wind velocity has been calculated for the grid points as follows:

$$F_g = \left\{ \frac{\sum_{i=1}^n \sum_{j=1}^m (W_{i,j} \times F_o)}{\sum_{i=1}^n \sum_{j=1}^m W_{i,j}} \right\} \quad W_{i,j} = \max \left\{ 0, \frac{(R^2 - r_{i,j}^2)}{(R^2 + r_{i,j}^2)} \right\} \quad (22)$$

where  $r_{i,j}$  is the distance between two points  $s$  (synoptic stations) and  $g$  (grid points),  $F_o$  is the data in  $m$  selected stations,  $F_g$  is the value of data determining in  $n$  grid points,  $R$  is influence radius and  $W_{i,j}$  is a weight function of the stations related to the grid points.

Table 6 Comparison of wind velocity by Cressman, analytical wind field and NOAA data

Item	Lat.	Lon.	Cressman analysis	Deviation (%)	Analytical wind field	Deviation (%)
1	28.00	51.00	1.350	8.6	1.79	17.8
2	27.50	51.00	1.362	20.8	1.72	0.0
3	27.00	50.00	1.336	15.4	1.38	14.5
4	27.00	52.00	1.167	31.0	2.12	19.8
5	26.50	51.00	1.371	20.3	1.56	10.2

In the near-field region of an oil spill, tidal currents can be of considerable importance. The tides in the Persian Gulf are complex, consisting of a variety of tidal types. The tide raising forces constituents are included of some principal constituents. For the sun-earth-moon system, there are so many tide-raising-force constituents. A number of 15 are related to lunar, 7 to solar and the rest are related to long-period and shallow water. Among these constituents such as diurnal, semi-diurnal, third-diurnal, fourth-diurnal, sixth-diurnal and long-term, four main constituents have been selected as below:

- Semi-diurnal  $M_2$  for the moon and  $S_2$  for the sun, periods of 12.42 [hr] and 12.00 [hr] respectively

- Diurnal  $K_1$  and  $O_1$  both for the moon, periods of 23.93 [hr] and 25.85 [hr] respectively

Mostly, other constituents have small amplitudes and often are not considerable. The weight of other constituents is about 1.5-2 % and is ignored here. In this work, four main constituents have been considered by using Admiralty method of tidal prediction NP 159-1969.

## 6 Oil transportation and decay

The total volume of the spilled oil as the pollutant is divided into discrete parcels. It is assumed that these parcels advect with the surrounding water body and diffuse as a result of random processes. The parcels are under the influence of the regular movement of the media with the velocity components  $(u, v, w)$  and turbulent fluctuations  $(u', v', w')$ . Therefore the coordinates  $X_k, Y_k$  and  $Z_k$  of particles in x, y, z directions are determined by:

$$X_k = X_k^0 + u \cdot \Delta t + [W_1]_{\mu=0}^{\sigma^2=1} \cdot \sqrt{2D_h \cdot \Delta t} \quad (23)$$

$$Y_k = Y_k^0 + [W_2]_{\mu=0}^{\sigma^2=1} \cdot \sqrt{2D_h \cdot \Delta t} \quad (24)$$

$$Z_k = Z_k^0 + w \Delta t + [W_3]_{\mu=0}^{\sigma^2=1} \sqrt{2D_v \cdot \Delta t} + 5.04 \left[ (\Delta \rho \cdot g \cdot \mu_w)^{1/3} / \rho_w^{2/3} \right] \cdot \Delta t \quad (25)$$

where the initial coordinates of the kth parcel are  $X_k^0, Y_k^0, Z_k^0$ . Velocity components  $(u, v)$  are determined by the dynamical field resulting Kelvin wave for each time interval.  $[W_1]_{\mu=0}^{\sigma^2=1}$ ,  $[W_2]_{\mu=0}^{\sigma^2=1}$  and  $[W_3]_{\mu=0}^{\sigma^2=1}$  are three independent random variables following reduced centered Gaussian distribution (i.e. of average zero and variance 1).  $D_h$  and  $D_v$  are horizontal and vertical dispersion coefficients. Vertical velocity  $w$  in the z direction has been determined by a Logarithmic profile:

$$w(z) = U_f \cdot \ln[30(h-z)/k_n], U_f = \left\{ V_{mean} \cdot \kappa / [\ln(30h/k_n) - 1] \right\} z < h \quad (26)$$

where  $z$  is the vertical co-ordinate measured from the sea surface and  $w(z)$  is the logarithmic current profile.  $\kappa$  is von Kármán's constant,  $k_n$  is Nikuradse roughness factor and  $U_f$  is friction velocity.  $V_{mean}$  is the mean current velocity determined based on Kelvin wave theory. Velocity fluctuations can be calculated based on the random walk technique. The component of the oil drop emergence  $w_b = g \cdot d_k^2 \cdot \Delta \rho / (18 \mu_w)$  and the droplet size  $d_k = 9.52 \mu_w^{2/3} / (g \cdot \rho_w \cdot \Delta \rho)^{1/3}$  are estimated by assuming the particle to be spherical and rigid and applying the force balance between the buoyancy and drag forces [17]. Where  $g$  is the gravity,  $\rho_o$  and  $\rho_w$  are oil and water density respectively and  $\Delta \rho$  is density difference.  $\mu_w$  is the water dynamic viscosity.

In this study, surface oil slick has been calculated due to gravitational-inertial-viscous and surface tension forces and also due to wind field [18] and surface oil slick due to shear dispersion has been calculated by [19]:

$$\frac{dA_k}{dt} = C_{k1} \cdot A_k^{0.33} \cdot (h_k)^{1.33} \quad (27)$$

where  $A_k$  represents the oil slick area and  $h_k$  stands for the oil slick thickness. The constant  $C_{k1}$  has been selected as 150 for the Persian Gulf.

Therefore, spreading, advection and dispersion are considered as oil transportation components and evaporation and emulsification as decay components. Dissolution has not been considered according to its order of magnitude was determined according to the method of Cohen [20]. The volume fraction of the oil evaporated is determined by a single component theory relation [21]. Under the influence of the wave action, water droplets may become entrained into the oil slick to form water-in-oil emulsions [22-23]. So, the volume fraction of evaporation ( $F_{ev}$ ) and the rate of the oil slick emulsification ( $F_{em}$ ) has been determined by:

$$F_{ev} = (\alpha_{ev} / C) \cdot [\ln P_0 + \ln(C \cdot K_E \cdot t + 1 / P_0)] \quad (28)$$

$$F_{em} = \left(1 - e^{-k_A k_B (1 + U_{wind-10m})^2 t}\right) / k_B \quad (29)$$

where,  $\alpha_{ev}$  is a correction coefficient,  $P_0$  is initial vapor pressure at temperature  $T_E$ .  $C$  has been calculated based on oil Index (API).  $k_E$  is  $0.0025 U_{wind-10m}^{0.78} A \cdot \nu / (R \cdot T \cdot V_0)$  and  $T$  is the temperature of oil.  $\nu$  is molar volume,  $R$  is gas constant. Also,  $K_A$  and  $K_B$  is constants and  $t$  is time. It is worth mentioning that sedimentation is not considered. In the surface layer and water column, decay can be expressed as the following respectively [24]:

$$Decay = -F_{ev} + F_{em} \quad (30)$$

$$Decay = F_{em} \quad (31)$$

## 7 Results

The water dynamical field has been obtained by two different hydrodynamic models. A portal containing wind velocity and direction, tidal main constituents, water surface level and water surface velocity is performed. Table (6), compares the wind velocities calculated by an analytical wind field and Cressman analysis with NOAA data at the spillage interval displaying fairly good conformity. The minimum error is in the northern part of the Persian Gulf showing 8.6 % and the maximum error is in the southern part of the Gulf. The maximum error is due to the lack of data near Arabian countries. Hence, an analytical wind field has been used not only because of the smaller amount of mean deviations on the whole grids, but also because of the possibility of time series generation. Table (7), compares the calculations and measurements of the main tidal constituents and water surface level using in Kelvin wave theory in four different locations such as Kish and Siri islands and Bandar-abbas and Bushehr ports. To verify the hydrodynamic model, calculations for water surface level and surface layer currents near Kish Island have been compared to the measured data. The computed water surface level and water surface velocity at Kish Island is compared with measured values [25]. It shows that the results present a successful speed-up procedure.

**Table 7** Comparison of tidal constituents for 4 locations in the Persian Gulf

Tidal constituents	M <sub>2</sub>		S <sub>2</sub>		K <sub>1</sub>		O <sub>1</sub>		Z <sub>0</sub>
	Ph	Amp.	Ph.	Amp.	Ph.	Amp.	Ph.	Amp.	
Max. Error %	15.2	14.1	21.1	27.5	19.8	18.4	20.7	23.4	18.9
Min. Error %	0.6	0.0	1.3	3.6	0.9	1.8	2.9	2.9	1.3

Applying the dynamical field, a semi stochastic oil spill model is built then. The model employs surface spreading, advection, evaporation and emulsification algorithms to determine transport and fate at the surface. Dissolution, as one of the decay components is ignored based on compared order of magnitude to other decay phenomena. Horizontal and vertical dispersions are simulated by random walk procedures. In Figure (4), oil slick thickness for time periods of 36 hours is compared with Chao et al.'s work. This result shows less oil slick thickness, due to the emulsification effects which have been considered in this work. In fact, in considering emulsification, oil disperses to water column sub layers close to surface and does not consider in surface layer. Figure (5) shows oil slick distribution in Z direction. It has been determined by a Logarithmic profile to show the effects of stochastic phenomena on vertical dispersion. Random numbers have been inserted in three positions such as diffusion, direction and diameter. Based on this distribution which is generated by two different methods i.e. prevailing wind by MIKE software and Weibull probability distribution using in Kelvin expansion, comparison of buoyancy effect is considered. Figure (6) shows a comparison of buoyancy effect for oil vertical dispersion. The results which have been provided using prevailing wind by Lonin [26] and Weibull distribution generated by this work are compared. It can be seen that, without buoyancy effect, oil droplets due to their mean diameters, have about 2-2.5 times more vertical dispersion in the water column. Therefore, regarding the buoyancy effect, calculations show a vertical dispersion in the water column 60% more than Lonin's prediction, while without buoyancy effect, the vertical dispersion is about 30% more than Lonin's. This difference is due to the consideration of evaporation and emulsification in this work. Lonin only used evaporation in his researches. The presence of emulsification effect causes more vertical dispersion due to the effect of heavy components.

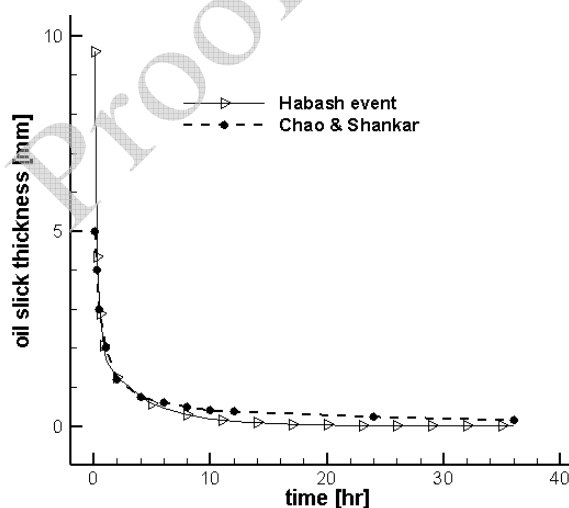


**Figure 4** Comparison of oil slick thickness

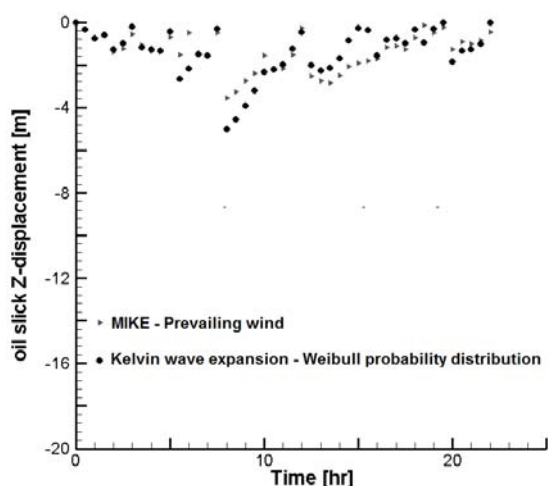


**Figure 5** Comparison of oil slick distribution in Z direction by Weibull distribution

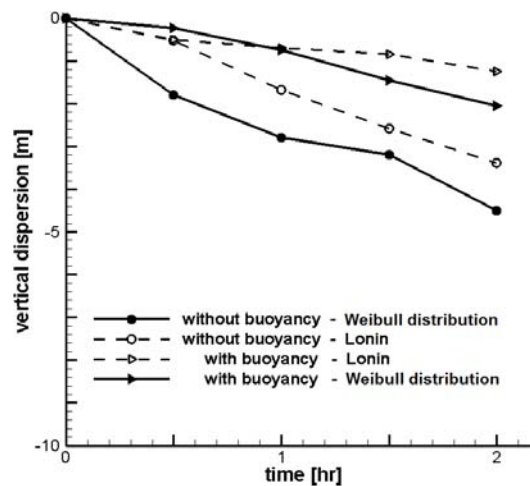


**Figure 6** Comparison of Buoyancy effect on vertical dispersion by Weibull distribution

Figures (7a) and (7b) show the comparison of oil slick trajectory with actual data for Habash and Nowruz oil spill event with fair agreement [5]. Therefore, as a final result in using Kelvin wave theory towards the speed up procedure, it is possible to determine a large number of results for prediction and providing risk assessment studies. In this regards, Figures (8), (9) show the time series of oil slick thickness during 1.5 days after release. They are prepared to show the effects of oil volume released on sea surface and oil type respectively. More initial released oil and heavier oil type (smaller API index) is caused more oil slick thickness which is predictable.

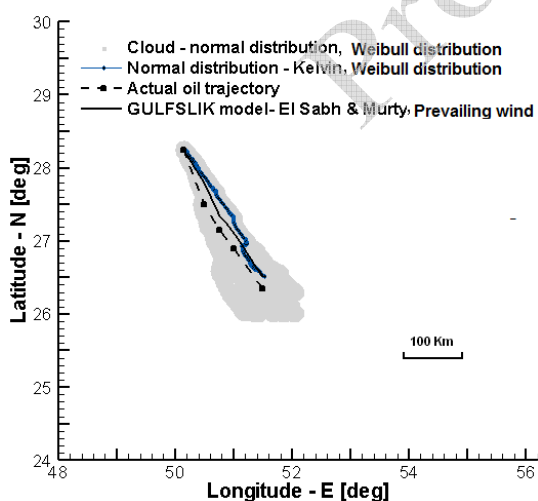


**Figure 7-a** Comparison of oil slick trajectory with actual data for Habash oil spill event

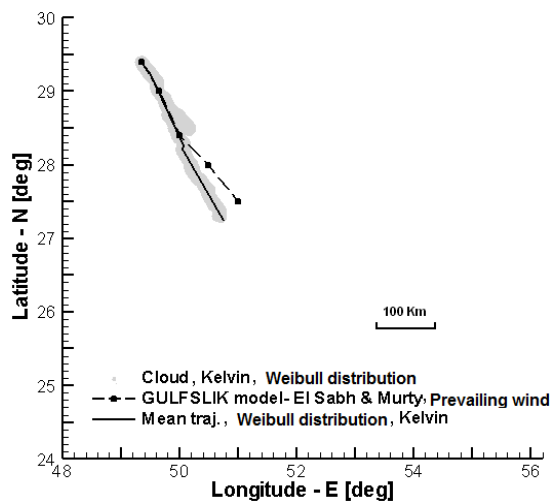


**Figure 7-b** Comparison of oil slick trajectory with actual data for Nowruz oil

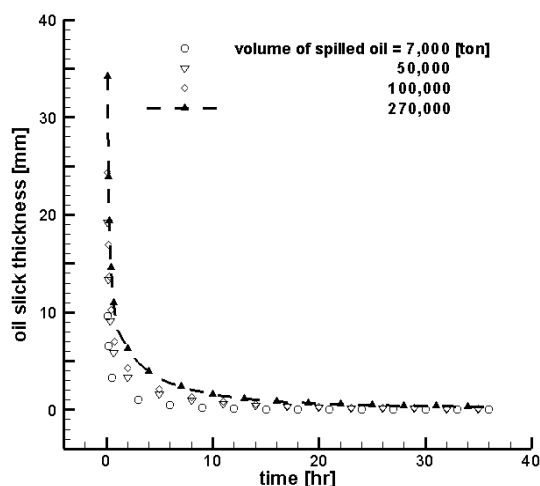


Figure 8 Oil volume effect on oil slick thickness

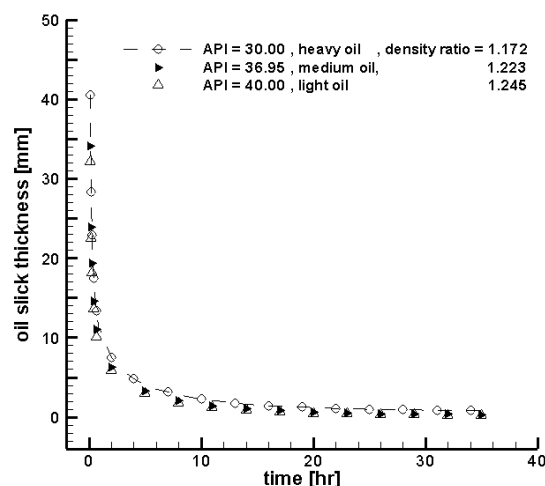


Figure 9 Density effect on oil slick thickness

## 8 Conclusion

An analytical wind field by using Weibull probability distribution is used to cover the lack of wind field time series. It is revealed that the region is located in shallow water range. The dynamical field estimated by a new hydrodynamic model. This model is developed to generate the dynamical field for the Persian Gulf. The model is presented to illustrate how the geostrophic approximation can be systematically exploited to produce a deterministic dynamical framework adequate for the calculation of motions of large time and space scales. Also it helps to study motions of oceanic relevance. This model shares the essential dynamical character of the geophysical system. By means of the Kelvin wave theory, it has been revealed in our previous studies that this new hydrodynamic calibration approach presents better results in short-term compared with an alternative hydrodynamic model in the Persian Gulf. This improvement is not only towards an estimation of the flow pattern in a simple manner, but also shows a successful speed-up procedure. This promotion is used as an application, to predict the trajectory of spilled oil, oil slick thickness and slick surface area along its trajectory. Therefore, capability of using an analytical wind field time series would be the main outcome. It facilitates the possibility of applying a simple and speedy method to provide oil spill hazard contour maps.

## References

- [1] Hockney, R.W., Estwood, J. W., "*Computer Simulation using Particles*", McGraw-Hill NY, pp. 640, New York, (1981).
- [2] Tkalich, P., Huda, K., and Hoong-Gin, K. Y., "A Multiphase Oil Spill Model", *J. Hydro. Res.*, Vol. 1, No. 2, pp. 115-125, (2003).
- [3] Hunter, J. R., "The Application of Lagrangian Particle-tracking Technique to Modeling of Dispersion in the Sea", *Numerical Modeling, Applications to Marine Sys.* pp. 257-269, (1987).

- [4] Najafi, H. S., Noye, B. J., and Teubne M. D., "Spherical-coordinate Numerical Model of the Persian Gulf", *Computation Techniques and Applications*", CTAC-95, World Scientific, Electronic Proceeding Publication, (1985).
- [5] El-Sabh, M. I., and Murty, T. S., "Simulation of the Movement and Dispersion of Oil Slicks in the Arabian Gulf", *Natural Hazards*, Vol. 1, pp. 197-219, (1988).
- [6] Al-Rabeh, A. H., Cekirge, H. M., and Gunay, N., "Modeling the Fate and Transportation of Al- Ahmadi Oil Spill", *Water Air and Soil Pollution*, Vol. 65, pp. 257-279, (1992).
- [7] Venkatesh, S., and Murty, T. S., "Numerical Simulation of the Movement of the 1991 Oil Spill in the Arabian Gulf", *Water Air and Soil Pollution*, Vol. 74, pp. 211-234, (1994).
- [8] Elshorbagy, W., and Elhakeem, A. A., "Risk Assessment Maps of Oil Spill for Major Desalination Plants in the United Arab Emirates", *Desalination*, Vol. 228, pp. 200-216 (2008).
- [9] Sabbagh-Yazdi, S., Zounemat, M., and Kermani, A., "Solution of Depth-averaged Tidal Currents in Persian Gulf on Unstructured Overlapping Finite Volumes", *International Journal for Numerical Methods in Fluids*, Vol. 55, pp. 81-101, (2007).
- [10] Elhakeem, A. A., Elshorbagy, W., and Chebbi, R., "Oil Spill Simulation and Validation in the Arabian (Persian) Gulf with Special Reference to the UAE Coast", *Water Air Soil Pollutant*, Vol. 184, pp. 243-254, (2007).
- [11] Elshorbagy, W., Azam, M., and Taguchi, K., "Hydrodynamic Characterization and Modeling of the Arabian Gulf", *Journal of Waterway, Port, Coastal and Ocean Eng.*, Vol. 132, No. 47, pp. 47-56, (2006).
- [12] Rakha, K., Al-Salem, K., and Neelamani, S., "Hydrodynamic Atlas for the Arabian (Persian) Gulf", *Journal of Coastal Research*, Special Issue, Vol. 50, pp. 550-554, (2007).
- [13] Komen, G. J., Cavaleri, L., Donelan, M., Hasselmann, K., Hasselmann, S., and Janssen, P.A.E.M., "*Dynamics and Modeling of Ocean Waves*", Cambridge University Press, pp. 156, (1995).
- [14] Pedlosky, J., "*Geophysical Fluid Dynamics*", 2<sup>nd</sup> edition, Springer-Verlag, pp. 75-80, New York, (1992).
- [15] Pugh, D. T., "Tides, Surges and Mean Sea-level", Natural Environment Research Council, Swindon, UK, John Wiley, (1996).
- [16] Wojtaszek, K., "Application of Transport Model for Building Contingency Maps of Oil Spills on the North Sea", Master Thesis, TUDELFT, Delft, (2003).
- [17] Zheng, L., Yapa, P.D., "Buoyant Velocity of Spherical and Non-spherical Bubbles/Droplets", *Journal of Hydraulic Engineering*, ASCE, November, Vol. 11, pp. 825-855, (2000).

- [18] Al-Rabeh, A. H., Cekirge, H. M., and Gunay, N., "A Stochastic Simulation Model of Oil Spill Fate and Transport", *Applied Mathematics Modeling*, Vol. 13, pp. 322-329, (1992).
- [19] Korotenko, K.A., Mamedov R.M., and Mooers C.N.K., "Prediction of the Dispersal of Oil Transport in the Caspian Sea Resulting from Continuous Release", *Spill Science & Tech. Bul*, Vol. 6, pp. 323-339, (2000).
- [20] Cohen, Y., Mackay, D., Shiu, W.Y., "Mass Transfer Rates between Oil Slicks and Water", *Journal of Chemical Engineering*, Vol. 58, pp. 569-574, (1980).
- [21] Mackay, D., Paterson, S. and Trudel, K., "A Mathematical Model of Oil Spill Behavior", *Environmental Protection Service, Fisheries and Environmental, Canada*, (1980).
- [22] Fingas, M., Fieldhouse, B., Lerouge, L., Lane, J., and Mullin, J., "Studies of Water-in-oil Emulsions: Energy and Work Threshold as a Function of Temperature", *Proceedings, 24th Arctic Marine Oil Spill Program Technical Seminar, Edmonton, Alberta, Environment, Canada*, (2001).
- [23] Xie, H., Yapa, P.D., and Nakata, K., "Modeling Eemulsification after an Oil Spill in the Sea", *Journal of Marine Systems*, Vol. 68, pp. 489-506, (2007).
- [24] Chao X., and Jothi Shankar N., "Two and Three Dimensional Oil Spill Model for Coastal Waters", *Ocean Engineering*, Vol. 28, pp. 1557-1573, (2001).
- [25] Badri, M.A., and Azimian, A. R., "An Oil Spill Model Based on the Kelvin Wave Theory and Artificial Wind Field for the Persian Gulf", *Indian Journal of Marine Sciences*, Vol. 39, No. 2, pp. 165-181, (2010).
- [26] Lonin, S. A., "Lagrangian Model for Oil Spill Diffusion at Sea", *Spill Science & Technology Bulletin*, Vol. 5, No. 5/6, pp. 331-336, (1999).

### Nomenclature

$A_p$	: a scaling parameter
$A_k$	: oil slick area
$C$	: calculated based on oil Index
$C_p$	: a dimensionless shape parameter
$C_0$	: wave velocity
$d_0$	: droplet size
$D_b$	: dissipated breaking wave energy per unit surface area
$D_h$	: horizontal dispersion coefficient
$D_v$	: vertical dispersion coefficient
$\Delta d$	: droplet size interval
<i>Decay</i>	: Oil decay fraction
$f(V)$	: Weibull probability density function
$F_g$	: determined wind data in grid points

$F_o$	: in selected synoptic stations
$F_{wc}$	: fraction of sea surface by breaking waves
$F_{ev}$	: volume fraction of evaporation
$F_{dis}$	: rate of the oil slick dissolution
$F_{em}$	: rate of the oil slick emulsification
$g$	: Gravity acceleration
$H_0$	: Basin depth-averaged
$h_k$	: oil slick thickness
$k_1, k_2, k_3$	: constants
$P_0$	: initial vapor pressure
$p(V)$	: cumulative Weibull probability distribution function of wind velocity
$Q$	: entrained mass of oil droplets
$R$	: real vector of probabilities
$R_1$	: calculated vector of probabilities
$S_{cov}$	: fraction of surface covered by oil
$S_2, K_1, M_2, O_1$	: tidal constituents
$T$	: water temperature
$u$	: determinant x-flow-velocity component
$u'$	: stochastic x-velocity component
$v$	: determinant y- flow-velocity component
$v'$	: stochastic y-velocity component
$U_f$	: friction velocity
$U_{wind-10m}$	: Wind velocity 10 meters above the sea level
$\bar{V}$	: mean value of wind field
$V_{mean}$	: mean current velocity
$W_1, W_2, W_3$	: normal random numbers
$W_{i,j}$	: weight function
$w(z)$	: z-velocity component
$x$	: x-direction coordinate
$x'$	: rotated x-direction coordinate
$X_k$	: slick position in x dir.
$X_k^0$	: initial slick position in x dir.
$y$	: y-direction coordinate
$y'$	: rotated y-direction coordinate
$Y_k$	: slick position in y dir.
$Y_k^0$	: initial slick position in y direction
$Z_0$	: mean water level
$Z_k$	: slick position in z dir.
$Z_k^0$	: initial slick position in z dir.

### Greek symbols

$\alpha_{ev}$	: a correction coefficient
$\varepsilon$	: least-squares function
$\phi_j$	: phase lag of main tidal constituents

$\Gamma$	:	Gamma function
$\eta$	:	water surface fluctuations
$\bar{\eta}(y)$	:	complex wave amplitude
$\tilde{\eta}$	:	water surface fluctuations after normalizing
$\eta_j$	:	water surface fluctuations of main tidal constituents
$\kappa$	:	von Kármán's constant
$\mu_w$	:	water viscosity
$\rho_w$	:	water density
$\rho_o$	:	oil density
$\sigma$	:	standard deviation of wind field
$\sigma^2$	:	variance of wind field

Proof Read

## چکیده

مهمترین منبع آلودگی های نفتی در خلیج فارس به حمل و نقل نفت توسط تانکرها و استخراج، تخلیه و انتقال نفت به وسیله پالایشگاه های فعال در بنادر مربوط می باشد. میدان دینامیکی آب توسط یک مدل هیدرودینامیکی جدید بدست آمده است. اثر میدان باد به عنوان نیروی رانش اصلی در انتقال و انتشار آلودگی های نفتی برای تعیین نحوه حرکت لکه نفت بر روی سطح آب با این مدل هیدرودینامیکی تلفیق شده است. توزیع چگالی احتمالی وی بول برای کالیبراسیون باد غالب از طریق داده های اندازه گیری بدست آمده و با سایر داده های میدانی مقایسه و انطباق خوبی ملاحظه شده است. برای مدلسازی پدیده جابه جایی و نفوذ در آبهای خلیج فارس به عنوان آبهای کم عمق از روش پیمایش اتفاقی استفاده شده است. مقایسه مسیر واقعی و محاسباتی بر اساس میدان باد گفته شده قابل قبول ارزیابی گردیده است.

Proof Read